IJMMM International Journal of Minerals, Metallurgy and Materials 矿物冶金与材料学报（英文版）

Electrochemical process for recovery of metallic Mn from waste $LiMn_2O_4$-based Li-ion batteries in NaCl–$CaCl_2$ melts

Jinglong Liang, Dongbin Wang, Le Wang, Hui Li, Weigang Cao, and Hongyan Yan

Cite this article as:
Jinglong Liang, Dongbin Wang, Le Wang, Hui Li, Weigang Cao, and Hongyan Yan, Electrochemical process for recovery of metallic Mn from waste $LiMn_2O_4$-based Li-ion batteries in NaCl–$CaCl_2$ melts, *Int. J. Miner. Metall. Mater.*, 29(2022), No. 3, pp. 473-478. https://doi.org/10.1007/s12613-020-2144-7

Articles you may be interested in

Hendrik Setiawan, Himawan Tri Bayu Murti Petrus, and Indra Perdana, Reaction kinetics modeling for lithium and cobalt recovery from spent lithium-ion batteries using acetic acid, *Int. J. Miner. Metall. Mater.*, 26(2019), No. 1, pp. 98-107. https://doi.org/10.1007/s12613-019-1713-0

Kai-lin Cheng, Dao-bin Mu, Bo-rong Wu, Lei Wang, Ying Jiang, and Rui Wang, Electrochemical performance of a nickel-rich $LiNi_{0.6}Co_{0.2}Mn_{0.2}O_2$ cathode material for lithium-ion batteries under different cut-off voltages, *Int. J. Miner. Metall. Mater.*, 24(2017), No. 3, pp. 342-351. https://doi.org/10.1007/s12613-017-1413-6

Dong Wang, Sheng Pang, Chun-yue Zhou, Yan Peng, Zhi Wang, and Xu-zhong Gong, Improve titanate reduction by electro-deoxidation of $Ca_3Ti_2O_7$ precursor in molten $CaCl_2$, *Int. J. Miner. Metall. Mater.*, 27(2020), No. 12, pp. 1618-1625. https://doi.org/10.1007/s12613-020-2165-2

Li-fan Wang, Meng-meng Geng, Xia-nan Ding, Chen Fang, Yu Zhang, Shan-shan Shi, Yong Zheng, Kai Yang, Chun Zhan, and Xin-dong Wang, Research progress of the electrochemical impedance technique applied to the high-capacity lithium-ion battery, *Int. J. Miner. Metall. Mater.*, 28(2021), No. 4, pp. 538-552. https://doi.org/10.1007/s12613-020-2218-6

Cheng Yang, Jia-liang Zhang, Qian-kun Jing, Yu-bo Liu, Yong-qiang Chen, and Cheng-yan Wang, Recovery and regeneration of $LiFePO_4$ from spent lithium-ion batteries via a novel pretreatment process, *Int. J. Miner. Metall. Mater.*, 28(2021), No. 9, pp. 1478-1487. https://doi.org/10.1007/s12613-020-2137-6

Zhi-yuan Feng, Wen-jie Peng, Zhi-xing Wang, Hua-jun Guo, Xin-hai Li, Guo-chun Yan, and Jie-xi Wang, Review of silicon-based alloys for lithium-ion battery anodes, *Int. J. Miner. Metall. Mater.*, 28(2021), No. 10, pp. 1549-1564. https://doi.org/10.1007/s12613-021-2335-x

IJMMM WeChat

QQ author group

International Journal of Minerals, Metallurgy and Materials
Volume 29, Number 3, March 2022, Page 473
https://doi.org/10.1007/s12613-020-2144-7

Electrochemical process for recovery of metallic Mn from waste $LiMn_2O_4$-based Li-ion batteries in NaCl−$CaCl_2$ melts

Jinglong Liang, Dongbin Wang, Le Wang, Hui Li✉, Weigang Cao, and Hongyan Yan

College of Metallurgy and Energy, North China University of Science and Technology, Tangshan 063210, China
(Received: 27 May 2020; revised: 9 July 2020; accepted: 14 July 2020)

Abstract: A new method is proposed for the recovery of Mn via the direct electrochemical reduction of $LiMn_2O_4$ from the waste of lithium-ion batteries in NaCl−$CaCl_2$ melts at 750°C. The results show that the $LiMn_2O_4$ reduction process by the electrochemical method on the coated electrode surface occurs in three steps: Mn(IV) → Mn(III) → Mn(II) → Mn. The products of this electro-deoxidation are $CaMn_2O_4$, MnO, $(MnO)_x(CaO)_{1-x}$, and Mn. Metal Mn appears when the electrolytic voltage increases to 2.6 V, which indicates that increasing the voltage may promote the deoxidation reaction process. With the advancement of the three-phase interline (3PI), electric deoxygenation gradually proceeds from the outer area of the crucible to the core. At high voltage, the kinetic process of the reduction reaction is accelerated, which generates double 3PIs at different stages.

Keywords: lithium-ion-battery waste; electrochemistry of melts; Mn recovery; electro-deoxidation; lithium manganate

1. Introduction

As one of the most popular energy storage devices, lithium-ion batteries (LIBs) have excellent performance and are widely used in power vehicles and electronic products [1−2], but there is a huge volume of waste LIBs produced every year. The efficient and environmentally friendly recycling of the valuable metals in the cathode materials of waste LIBs has attracted interest as a way to both reduce environmental pollution and recover valuable metals. To date, reasearch has mainly focused on hydrometallurgy [3−7], mechanical separation [8], and comprehensive recycling [9], with other reasearchers focusing on recycling and crystal regeneration [10−11].

Electrochemical methods for melts have made significant progress with respect to the reduction of metals such as Ti [12−16] and Si [16−19]. Many recycling methods have been developed, including the FFC-Cambridge [12] and USTB [13] processes, which have excellent performance in metal-oxide reduction and the recycling of metal-containing solid waste [20−25]. Zhang *et al.* [26] recycled the metals Co and Li from the $LiCoO_2$-battery cathode material in K_2CO_3−Na_2CO_3 melts. Compared with cobalt resources, the economic benefit of recycling manganese resources is lower, but as a solid waste, the direct disposal of manganese resources does not meet resource recovery requirements. As a heavy metal, manganese also requires effective treatment to reduce and eliminate its environmental impact. Alkaline earth metal chlorides have often been used in metal electrochemical processes due to their wide electrochemical windows and good stability [27]. Researchers have recycled Si, Ti, Fe, and other metals in the NaCl−$CaCl_2$ melts system, which has laid a foundation for further study [28−30]. In this study, we investigated the process of electrochemically reducing manganese from $LiMn_2O_4$ in equimolar NaCl−$CaCl_2$ melts, and obtained the electrochemical reduction mechanism and electrolytic conditions necessary for recycling manganese. The results of this work provide a theoretical basis for the green recycling of LIBs.

2. Experimental

The reagents in the experiment included NaCl (Sinopbarm Chemical Reagent, Co., Ltd., China, analytical grade), $CaCl_2$ (Sinopbarm Chemical Reagent, Co., Ltd., China, analytical grade), and $LiMn_2O_4$ (Wuxi Jewel Power & Materials Co., Ltd., China, ≥99.95%), which were dehydrated prior to the experiment. We thoroughly mixed 200 g of NaCl−$CaCl_2$ powder in an equimolar ratio and placed it into a corundum crucible. The melts were heated to 1023 K and maintained at that temperature for 1 h. All the experiments conducted in the resistance furnace were conducted under the protection of a high-purity argon atmostphere (Ar, 99.999%).

For the electrochemical analysis, which was performed at an electrochemical workstation (CHI660E, CH Instryment, Inc.), we used a three-electrode system, with a high-purity graphite rod (diameter (d) = 5 mm) as the counter electrode, an Ag/AgCl electrode as the reference electrode, and a Pt

✉ Corresponding author: Hui Li E-mail: lh@ncst.edu.cn

wire (d = 0.5 mm) coated with $LiMn_2O_4$ powder or not as the working electrode. We put 3 g of $LiMn_2O_4$ powder into 10 mL of absolute ethanol and subjected it to vibration by ultrasonic wave for 15 min to fully disperse the powder in the ethanol. The Pt wire was inserted into the mixture and then taken out and dried, and this process was repeated three to four times to evenly coat the surface of the Pt wire with the powder. The illustration of the electrolysis equipment was shown in Fig. 1.

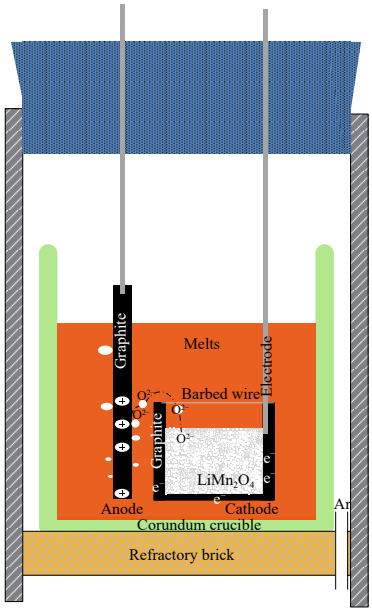

Fig. 1. Illustration of the electrolysis equipment.

Constant potential deoxygenation analysis was performed using a direct current power supply (GWINSTEK PSM-3004). In the constant-voltage deoxidation process, we used a two-electrode system with a high-purity graphite sheet as the anode. For the cathode, we used a graphite crucible (outer diameter 15 mm, inner diameter 8 mm, and depth 12 mm) wrapped with 400#-mesh barbed wire and filled with 0.8 g of $LiMn_2O_4$ powder.

After deoxygenation, the electrode was taken out and the water was cooled. The product was separated from the graphite crucible and cleaned by ultrasonic wave in a water bath at 0°C. The products were analyzed by X-ray diffraction (XRD, Noran7 Thermo Fisher), scanning electron microscopy (SEM, PHENOM ProX), and energy-dispersive X-ray spectroscopy (EDS, PHENOM ProX).

3. Results and discussion

3.1. Cell voltage electrolysis analysis

To study the effect of voltage on the $LiMn_2O_4$ reduction process, the electro-oxidation voltage range was varied from 0.5 to 3.0 V at 750°C for 12 h, the results of which are shown in Fig. 2(a). At 0.5 V, the main products were $CaMn_2O_4$ and a little MnO. At 2.5 V, the products comprised two solid solutions, $(MnO)_{0.614}(CaO)_{0.386}$ and $(MnO)_{0.253}(CaO)_{0.747}$. In this electrolytic condition, Mn(III) could be completely reduced to Mn(II), and $CaMn_2O_4$ completely disappeared. Solid solutions were produced by the deoxidation of $CaMn_2O_4$. At 2.6 V, metal manganese appeared and calcium oxide (CaO) and calcium hydroxide ($Ca(OH)_2$) formed. CaO was produced by the deoxidation of the solid solution, and the formation of $Ca(OH)_2$ was due to the hydrolysis of CaO during the process of washing in deionized water [31]. At 3.0 V, no manganese oxide could be detected in the products, only metal manganese, CaO, and $Ca(OH)_2$. Thus, the reaction was determined by the electrolytic voltage and the reactions proceeded when the voltage reached certain reaction conditions.

Under the influence of voltage, Ca^{2+} exhibited directional movement in the melts, and accumulated around $LiMn_2O_4$, with Mn(IV) converting to Mn(III) upon the formation of $CaMn_2O_4$.

Fig. 2(b)–(e) shows photos of the electrolytic products at different potentials. Fig. 2(b) shows the product produced at 0.5 V, wherein that in contact with the crucible was green, and those in the interior of the crucible were black. At 2.5 V, all the products were completely green, as shown in Fig. 2(c). According to the results shown in Fig. 2(b), at 0.5 V, no $CaMn_2O_4$ was present, a divalent manganese compound was the main component, the black product was $CaMn_2O_4$, and the green product was MnO. As shown in Fig. 2(d), at 2.6 V, the product changed from green to dark gray, with just a small amount of green product at the bottom of the crucible. According to the result shown in Fig. 2(a), the green product was the incompletely reduced MnO and the dark gray mater-

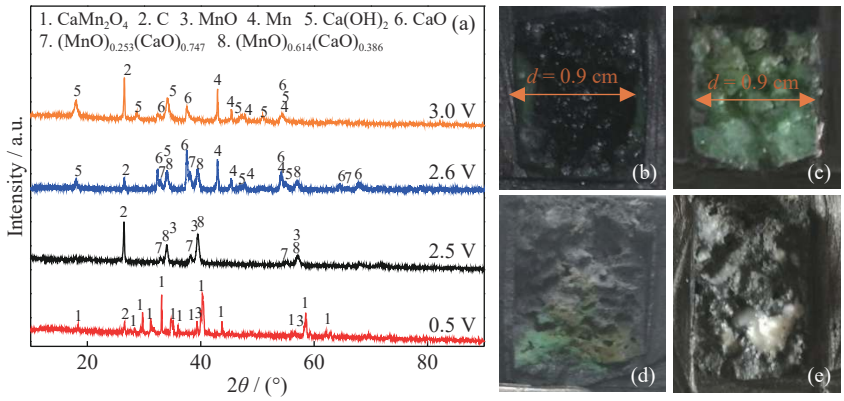

Fig. 2. Electro-deoxidation products at different voltages for 12 h: (a) XRD results; photos of products at (b) 0.5 V, (c) 2.5 V, (d) 2.6 V, and (e) 3.0 V.

ial was metal Mn. At 3.0 V, the product was completely dark gray, which, according to Fig. 2(a), was metal Mn with a small quantity of Ca compound. During the electro-deoxidation process, at 2.5 V, the product was green MnO, and the MnO was not reduced to manganese due to the limited voltage. The deoxygenation reaction stagnates when the reaction of Mn(II) to metal manganese cannot be driven by the electrical conditions. When the voltage was increased to 2.6 V and higher, the conversion of MnO to metal manganese was promoted.

As shown in Fig. 3, the deoxygenation time of reaction 1 (R1) and reaction 2 (R2) at 3.0 V is less than that at 2.6 V. For 2 h, the electro-deoxidation of $LiMn_2O_4$ entered the reaction 3 (R3) step at 3.0 V, but the electro-deoxidation time is longer at 2.6 V. Combined with the XRD results, it is evident that the $LiMn_2O_4$ is completely deoxidized at 3.0 V for 12 h, but $LiMn_2O_4$ is not completely deoxidized at 2.6 V. The speed of the reaction also increased when the voltage is increased. However, excessive voltage increases energy consumption and cost.

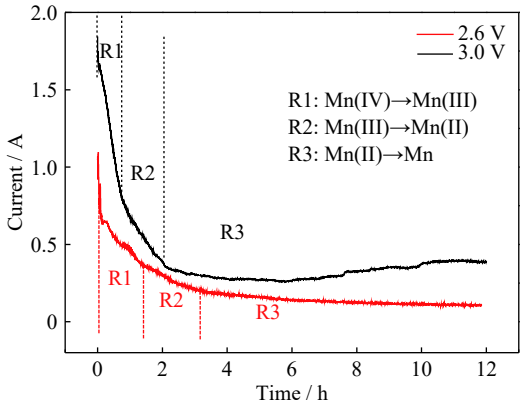

Fig. 3. Current data for electro-deoxidation over 12 h at 2.6 and 3.0 V.

The charge of the electrical deoxidation process can be obtained using Eq. (1).

$$Q = \int_{t_1}^{t_2} I\mathrm{d}t \tag{1}$$

where Q is the charge consumption (C), I is the current (A), t_1 and t_2 are the start and end time of the reaction (s). The calculations reveal that a 17509 charge was consumed in the electro-deoxidation process for 12 h at 3.0 V, the work expended during the reduction was 4.377 kJ, and the energy consumption was 0.12×10^{-2} kW·h. In the experiment, the mass of $LiMn_2O_4$ was 0.8 g and that of manganese was 0.48 g. To obtain 1 t of metal manganese required 2500 kW·h of electricity by electrical deoxidation.

The deoxidation process of $LiMn_2O_4$ mainly includes the following steps. First, spinel lithium manganate ($LiMn_2O_4$) is decomposed to produce $CaMn_2O_4$, MnO, and O_2 in melts at 750°C. Next, Mn(III) is deoxidized to Mn(II). Third, the divalent manganese oxide and its solid solution are deoxidized together to obtain metal manganese. The total reduction process of manganese is expressed as follows: Mn(IV)→ Mn(III)→ Mn(II)→ Mn.

Reaction of cathode:

$$LiMn_2O_4 + Ca^{2+} + e^- = CaMn_2O_4 + Li^+ \tag{2}$$

$$CaMn_2O_4 + 2e^- = 2MnO + CaO + O^{2-} \tag{3}$$

$$MnO + 2e^- = Mn + O^{2-} \tag{4}$$

Reaction of anode:

$$O^{2-} + C = CO_2 + 2e^- \tag{5}$$

To study the green material in the reaction process, we identified the products at 0.5 V for 12 h, the results of which are shown in Fig. 4. As evident in the figure, there are clear boundary layers, in which the uppermost layer is the graphite crucible, the green product near the graphite crucible is MnO, and the bottom layer is the incompletely reduced product $CaMn_2O_4$. The reaction process gradually proceeded from the $LiMn_2O_4$ material in contact with the crucible to that inside the crucible.

3.2. Time analysis

The effect of the reaction time on the $LiMn_2O_4$ deoxidation process was studied at 3.0 V and 750°C, the XRD results of which are shown in Fig. 5(a). For 0.5 h, the deoxidation products included $CaMn_2O_4$, MnO, and a little $(MnO)_{0.252}(CaO)_{0.748}$. The characteristic peaks of $CaMn_2O_4$ decreased, and the solid solutions $(MnO)_{0.252}(CaO)_{0.748}$ and $(MnO)_{0.877}(CaO)_{0.123}$ appeared for 2 h, which indicated that $CaMn_2O_4$ had continued to be reduced during this stage, with peaks of metal manganese also appearing in the products. Therefore, different stages of electrical deoxidation occurred simultan-

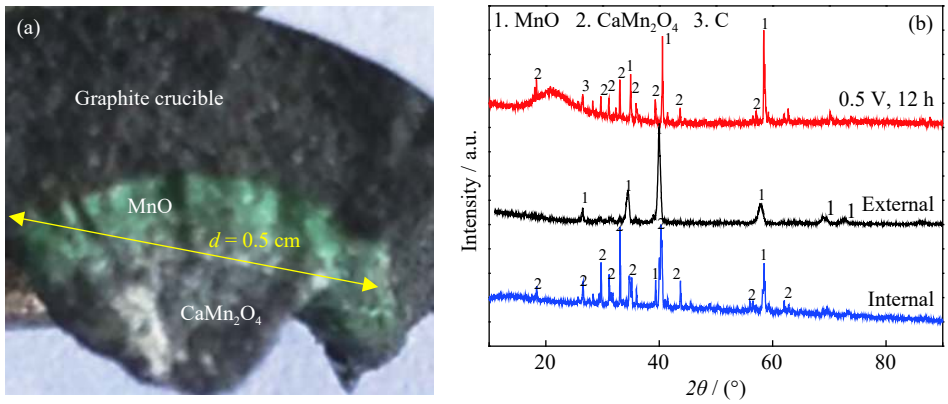

Fig. 4. (a) Sectional view of the electrical deoxidation product and (b) XRD test results at 0.5 V for 12 h.

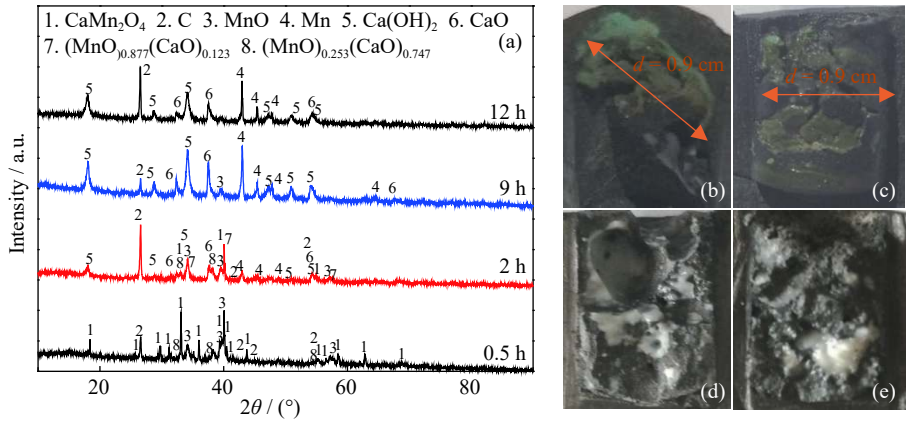

Fig. 5. Electro-deoxidation products at 3.0 V for different times: (a) XRD results; (b) photos of products for (b) 0.5 h, (c) 2 h, (d) 9 h, and (e) 12 h.

eously in the melts when driven by a high electrical force, but $CaMn_2O_4$ had not been completely reduced to MnO. With increased deoxidation time, the manganese oxide was continuously reduced, with a small amount of MnO detected for 9 h. The manganese had been completely reduced for 12 h.

Fig. 5(b)–(e) shows the electro-deoxidation products at different times. At 3.0 V, the interior of the product was black, with green parts apparent only where the melts, crucible, and $LiMn_2O_4$ were in contact for 0.5 h. From the XRD analysis in Fig. 5(a), we know that the green product was MnO and the black product was $CaMn_2O_4$. In Fig. 5(c), we can see that most of the products were green, and only a small amount was still black for 2 h. The products changed to dark gray from green for 9 h. According to the XRD results in Fig. 5(a), the dark gray products were mainly composed of metal manganese and the volume of the deoxygenated product had been significantly reduced relative to the intermediate product. As shown in Fig. 5, metal manganese was detected in the product for 3.0 V. The SEM, EDS, and element distribution chart of deoxygenated products are shown in Fig. 6. Based on the combined results obtained by SEM and EDS, we can conclude that elements Mn and O were detected on the surface of the product, and their quality was excellent.

In Fig. 7, during the deoxidation from $LiMn_2O_4$ to the metal Mn at a voltage of 3.0 V, the initial reaction only occurred at the three-phase interline (3PI), where the oxide interface, melts interface, and graphite crucible were in contact [30]. After the manganese oxide had been deoxidized, the reaction moved to the next material that could be deoxidized, which means the electrical deoxidation process in the melts proceeded gradually. With the deepening of the reaction process, the reduced products gradually aggregated and the 3PI continued to advance. At the same time, the MnO product obtained in the first step continued to be reduced to metal manganese, for which there appeared a new 3PI. With the deepened new 3PI, subsequent deoxidation and continuous metallization processes occurred. This meant there were three layers of different substances: the innermost layer was the product not yet having undergone a deoxidation reaction, the second outer layer was the MnO product from the first-stage reduction process, and the outermost layer was the reduced metal manganese. When the diffusion of the melts was unsatisfactory in the deoxidizer, the development of the 3PI and the reaction process were severely hindered, the deoxygenation rate was reduced, and the deoxygenation process could not be completely finished [30]. These effects were reduced when the oxide powder was deoxidized in the graphite crucible, because the gap between the powders was conducive to the formation of the 3PI.

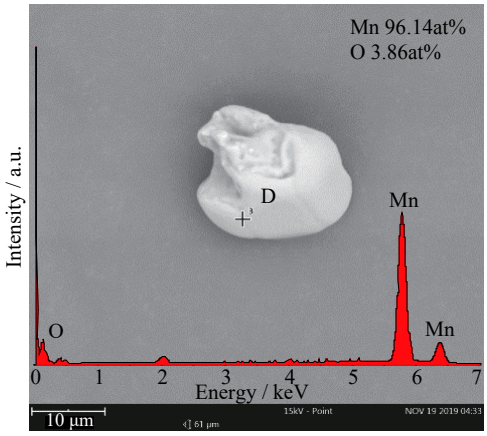

Fig. 6. SEM of electro-deoxidation product Mn at 3.0 V for 12 h. Inset: EDS spectrum of point D.

3.3. Cyclic voltammetry on platinum-coated electrode

Fig. 8 shows the cyclic voltammetry curve of $LiMn_2O_4$ with the Pt-coated electrode at 750°C in the NaCl–$CaCl_2$ system. In Fig. 8(a), the blue line is the scan result with the uncoated electrode and the red line is the scan result of the coated electrode. In the electrochemical window of pure melts, the cyclic voltammetry curve of $LiMn_2O_4$ shows three clear redox peaks. Fig. 8(b) shows the multi-cycle cyclic voltammetry scan with the coated electrode. In the reduction process of the first reverse scan, three obvious reduction peaks appeared, peak *a*, peak *b*, and peak *c*, in the range of −0.3 to −0.7 V. Peak *a* was produced by the $LiMn_2O_4$ reduction process from Mn(IV) to Mn(III), with the products in this process in the form of the more thermodynamically stable $CaMn_2O_4$. Peak *b* was caused by the $CaMn_2O_4$ reduction process from Mn(III) to Mn(II). From the electric deoxidation process at different voltages in Fig. 2, we can see that

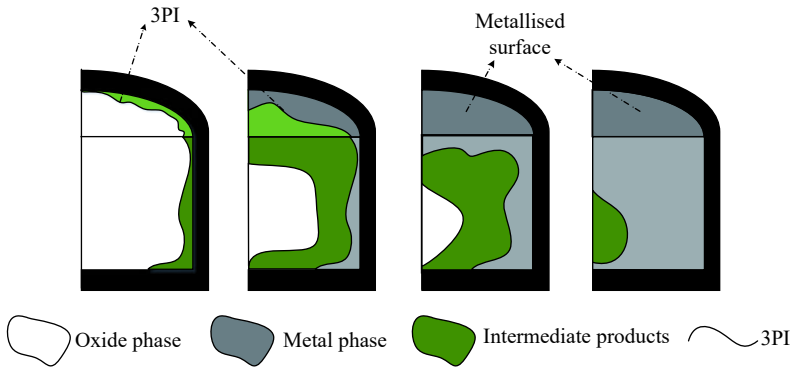

Fig. 7. Schematic of simultaneous reduction at high voltage.

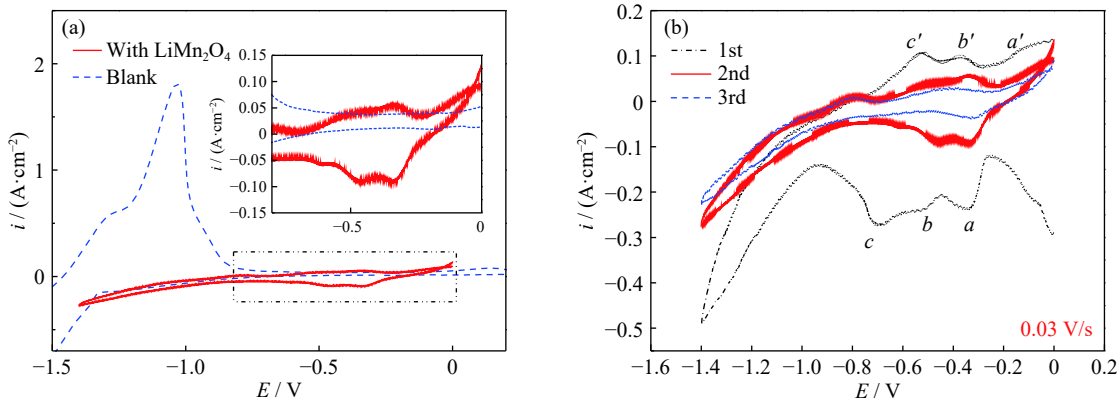

Fig. 8. Cyclic voltammetry curves of Pt-coated electrode surface (T = 750°C, reference coating: Ag/AgCl): (a) comparison of coated or uncoated electrode; (b) cyclic voltammograms of multi-turn scanning.

the deoxidation rate of $CaMn_2O_4$ was slowly. In that case, reduction peak *b* also showed a gentle trend during the electrochemical test. Peak *c* shows the reduction process of Mn(II) to metal Mn, which corresponded to the reduction process of MnO to metal Mn in the constant-voltage deoxidation process. During the forward scan, peak *c*′, peak *b*′, and peak *a*′ appeared in the range of −0.6 to 0 V, in which the metal Mn was reoxidezed. Peak *c*′ was caused by the reoxidation to Mn(II) from the reduced metal Mn, and peak *b*′ was the reverse process of peak *b*, whereby Mn(II) was oxidized to Mn(III). Due to the effect of Ca^{2+} in melts, the oxidation product was $CaMn_2O_4$. Finally, Mn(III) was oxidized to Mn(IV), which appeard as peak *a*′ in the electrical signal. In another reverse scan, three clear reduction peaks appeared in the cyclic voltammetry results in which, compared with the reduction peaks of the first cycle, the current density values were significantly reduced. The product in the oxidation process did not completely return to the electrode surface, which resulted in a reduction of the active particles on the electrode surface [32]. Furthermore, the peak current in the oxidation and reduction processes gradually weakened. The more redox processes occur, the less active are the particles on the electrode surface. Therefore, in the cyclic voltammetry process, the peak current gradually weakens as the number of cycles increases.

4. Conclusions

We systematically investigated the effects of voltage and time on the electrochemical reduction mechanism of manganese in $LiMn_2O_4$ in an NaCl–$CaCl_2$ melts system with an equimolar ratio at 750°C. Based on our results, we can make the following conclusions.

(1) Metal Mn can be obtained by the constant-voltage deoxidation of $LiMn_2O_4$ at 2.6 V, and the deoxygenation process can be accelerated by increasing the voltage.

(2) The first step of the deoxygenation process proceeds from the outer area to the inside to produce Mn(II), which continues to reduce, thereby forming two reaction interfaces.

(3) Cyclic voltammetry results reveal that the process of reducing $LiMn_2O_4$ to metal manganese on a Pt-coated electrode surface occurs in three steps: Mn(IV) → Mn(III) → Mn(II) → Mn.

Acknowledgements

This work was financially supported by the National Natural Science Foundation of China (No. 51774143).

Conflict of Interest

The authors declare no conflict of interest.

References

[1] P.Y. Guan, L. Zhou, Z.L. Yu, Y.D. Sun, Y.J. Liu, F.X. Wu, Y.F. Jiang, and D.W. Chu, Recent progress of surface coating on cathode materials for high-performance lithium-ion batteries, *J. Energy Chem.*, 43(2020), p. 220.

[2] Y.N. Xu, Y.Y. Dong, X. Han, X.F. Wang, Y.J. Wang, L.F. Jiao, and H.T. Yuan, Application for simply recovered $LiCoO_2$ material as a high-performance candidate for supercapacitor in aqueous system, *ACS Sustainable Chem. Eng.*, 3(2015), No. 10, p. 2435.

[3] G.L. Gao, X.M. Luo, X.Y. Lou, Y.G. Guo, R.J. Su, J. Guan, Y.S. Li, H. Yuan, J. Dai, and Z. Jiao, Efficient sulfuric acid-Vitamin C leaching system: Towards enhanced extraction of cobalt from spent lithium-ion batteries, *J. Mater. Cycles Waste Manage.*, 21(2019), No. 4, p. 942.

[4] L. Li, Y.F. Bian, X.X. Zhang, Y. Yao, Q. Xue, E. Fan, F. Wu, and R.J Chen, A green and effective room-temperature recycling process of $LiFePO_4$ cathode materials for lithium-ion batteries, *Waste Manage.*, 85(2019), p. 437.

[5] M. Roshanfar, R. Golmohammadzadeh, and F. Rashchi. An environmentally friendly method for recovery of lithium and cobalt from spent lithium-ion batteries using gluconic and lactic acids, *J. Environ. Chem. Eng*, 7(2019), No. 1, art. No. 102794.

[6] H. Setiawan, H. T. B. M. Petrus, and I. Perdan, Reaction kinetics modeling for lithium and cobalt recovery from spent lithium-ion batteries using acetic acid, *Int. J. Miner. Metall. Mater.*, 26(2019), No. 1, p. 98.

[7] X.P. Chen, D.Z. Kang, L. Cao, J.Z. Li, T. Zhou, and H.R. Ma, Separation and recovery of valuable metals from spent lithium ion batteries: Simultaneous recovery of Li and Co in a single step, *Sep. Purif. Technol.*, 210(2019), p. 690.

[8] J.F. Xiao, J. Li, Z.Q. Xu, Recycling metals from lithium ion battery by mechanical separation and vacuum metallurgy, *J. Hazard. Mater.*, 338(2017), p. 124.

[9] W.Y. Wang, C.H. Yen, J.L. Lin, and R.B. Xu, Recovery of high-purity metallic cobalt from lithium nickel manganese cobalt oxide (NMC)-type Li-ion battery, *J. Mater. Cycles Waste Manage.*, 21(2019), No. 2, p. 300.

[10] Q. Liang, H.F. Yue, S.F. Wang, S.Y. Yang, K. Lam, and X.H. Hou, Recycling and crystal regeneration of commercial used $LiFePO_4$ cathode materials, *Electrochim. Acta*, 330(2020), art. No. 135323.

[11] Y. Zhou, W. Shan, S.F. Wang, K. Lam, Q. Ru, F.M. Chen, and X.H. Hou, Recovery Li/Co from spent $LiCoO_2$ electrode based on an aqueous dual-ion lithium-air battery, *Electrochim. Acta*, 332(2020), art. No. 135529.

[12] G.Z. Chen, D.J. Fray, T.W. Farthing, Direct electrochemical reduction of titanium dioxide to titanium in molten calcium chloride, *Nature*, 407(2000), No. 6802, p. 361.

[13] S.Q. Jiao and H.M. Zhu, Electrolysis of Ti_2CO_3 solid solution prepared by TiC and TiO_2, *J. Alloys Compd.*, 438(2007), No. 1-2, p. 243.

[14] D.S. Maha Vishnu, N. Sanil, L. Shakila, R. Sudha, K.S. Mohandas, and K. Nagarajan, Electrochemical reduction of TiO_2 powders in molten calcium chloride, *Electrochim. Acta*, 159(2015), p. 124.

[15] X.Y. Liu, M.L. Hu, C.G. Bai, and X.W. Lv, Effect of electrical conductivity and porosity of cathode on electro-deoxidation process of ilmenite concentrate, *Rare Met. Mater. Eng.*, 46(2017), No. 5, p. 1176.

[16] H.D. Jiao, Q.Y. Wang, J.B. Ge, H.B. Sun, and S.Q. Jiao, Electrochemical synthesis of Ti_5Si_3 in $CaCl_2$ melt, *J. Alloys Compd.*, 582(2014), p. 146.

[17] X. Yang, L. Ji, X.L. Zou, T. Lim, J. Zhao, E.T. Yu, and A.J. Bard, Toward cost-effective manufacturing of silicon solar cells: electrodeposition of high-quality Si films in a $CaCl_2$-based melts, *Angew. Chem.*, 56(2017), No. 47, p. 15078.

[18] Y. Sakanaka, and T. Goto, Electrodeposition of Si film on Ag substrate in molten LiF–NaF–KF directly dissolving SiO_2, *Electrochim. Acta*, 164(2015), p. 139.

[19] Y. Sakanaka, A. Murata, T. Goto, and K. Hachiya, Electrodeposition of porous Si film from SiO_2 in molten $BaCl_2$−$CaCl_2$−NaCl, *J. Alloys Compd.*, 695(2017), p. 2131.

[20] W. Weng, M.Y. Wang, X.Z. Gong, Z. Wang, D. Wang, and Z.C. Guo, Electrochemical reduction behavior of soluble $CaTiO_3$ in Na_3AlF_6−AlF_3 melt for the preparation of metal titanium, *J. Electrochem. Soc.*, 164(2017), No. 9, p. D551.

[21] L. Kartal, M. B. Daryal, G. K. Şireli, and S. Timur. One-step electrochemical reduction of stibnite concentrate in molten borax, *Int. J. Miner. Metall. Mater.*, 26(2019), No. 10, p. 1258.

[22] W. Weng, M.Y. Wang, X.Z. Gong, Z.Wang, D. Wang, and Z.C. Guo, Direct electro-deposition of metallic chromium from K_2CrO_4 in the equimolar $CaCl_2$−KCl melts and its reduction mechanism, *Electrochim. Acta*, 212(2016), p. 162.

[23] L. Wang, W.Z. Liu, J.P. Hu, Q. Liu, H.R Yue, B. Liang, G.Q. Zhang, D.M. Luo, H.P. Xie, and C. Li, Indirect mineral carbonation of titanium-bearing blast furnace slag coupled with recovery of TiO_2 and Al_2O_3, *Chin. J. Chem. Eng.*, 26(2018), No. 3, p. 583.

[24] X.L. Ge, X.D. Wang, and S. Seetharaman, Copper extraction from copper ore by electro-reduction in molten $CaCl_2$–NaCl, *Electrochim. Acta*, 54(2009), No. 18, p. 4397.

[25] L. Kartal and S. Timur, Direct electrochemical reduction of copper sulfide in molten borax, *Int. J. Miner. Metall. Mater.*, 26(2019), No. 8, p. 992.

[26] B.L. Zhang, H.W. Xie, B.H. Lu, X. Chen, P.F. Xing, J.K. Qu, Q.S. Song, and H.Y. Yin, A green electrochemical process to recover Co and Li from spent $LiCoO_2$-based batteries in meltss, *ACS Sustainable Chem. Eng.*, 7(2019), No. 15, p. 13391.

[27] H. Li, D.B. Wang, J.L. Liang, H.Y. Yan, Z.Y. Cai, and R.G. Reddy, Electrochemical mechanism for the preparation of Fe−Si alloys by melts electrodeposition, *Int. J. Chem. React. Eng.*, 18(2019), No. 2, art. No. 20190112.

[28] J.L. Liang, H. Li, D.X. Huo, H.Y. Yan, R.G. Reddy, L.G. Wang, and L.Q. Wang, Electrochemical characteristics of TiO_2 in NaCl−KCl−NaF melts system, *Ionics*, 24(2018), No. 10, p. 3221.

[29] H. Li, L.S. Zhang, J.L. Liang, R.G. Reddy, H.Y. Yan, and Y.H. Yin, Electrochemical Behavior of Fe_3O_4 in NaCl−$CaCl_2$ Melts, *Int. J. Chem. React. Eng.*, 17(2019), No. 10, art. No. 0190017.

[30] G.Z. Chen and D.J. Fray, Understanding the electro-reduction of metal oxides in molten salts, [in] *Light Metals Symposium*, Charlotte, NC, 2004, p. 881.

[31] W. Weng, M.Y. Wang, X.Z. Gong, and Z.C. Guo, Thermodynamic analysis on the direct preparation of metallic vanadium from $NaVO_3$ by molten salt electrolysis, *Chin. J. Chem. Eng.*, 24(2016), No. 5, p. 671.

[32] D.Y. Tang, H.Y. Yin, W. Xiao, H. Zhu, X.H. Mao, and D.H. Wang, Reduction mechanism and carbon content investigation for electrolytic production of iron from solid Fe_2O_3 in molten K_2CO_3–Na_2CO_3 using an inert anode, *J. Electroanal. Chem.*, 689(2013), p. 109.